The role of geometry changes and debris formation associated with wear on the temperature field in fretting contacts

X. Jin, W. Sun, P.H. Shipway

Faculty of Engineering, University of Nottingham, Nottingham, UK

Abstract

The temperature of a fretting contact is known to be a key factor in its development. However, as a test proceeds, the wear scar changes, both geometrically and through the formation of oxide-based debris-beds. Accordingly, the effects of these on the near-surface temperature field resulting from frictional heating in fretting has been analysed via numerical modelling. Under the test conditions examined, it was predicted that (i) the development of the wear scar geometry would result in a significant (up to ~ 25%) reduction in the mean-surface temperature rise, and (ii) the formation of a typical oxide debris bed would result in a significant (up to ~ 80%) increase in the mean-surface temperature rise.

Keywords: frictional heating, stainless steel, 304, finite element modelling, FE

Nomenclature

b	elastic half-width of the contact	$s(t)$	the position of the moving origin
C	specific heat capacity	t	time
$D(\alpha, t)$	the distance from a chosen point within the contact to a defined point in the body	T	environment temperature
E^c	Young's moduli of the cylindrical specimen	v^c	Poisson's ratios of the cylindrical specimen
E^f	Young's moduli of the flat specimen	v^f	Poisson's ratios of the flat specimen
E^*	composite modulus of the two contacting bodies	$v(t)$	sliding velocity
E_d	dissipated energy per cycle	W	length of the contact
f	frequency of fretting	(x', y')	a defined point in the body
F_f	frictional force	α	distance from the centre of the heat source
k	thermal conductivity	γ	the Euler constant = 0.5772…
O	fixed origin	δ	slip amplitude
O'	moving origin	Δ	applied displacement
P	normal load	Δ^*	applied displacement amplitude
P'	normal load per unit length	δT	temperature rise from an instantaneous line heat source
p_0	maximum contact pressure	$\delta\bar{T}$	average temperature rise from a constant heat input rate
$p(\alpha)$	contact pressure	ΔT	temperature rise from the moving fretting frictional heat source
$Q(t)$	overall power of the heat source	$\Delta\bar{T}$	temperature rise from the static

			constant fretting frictional heat source
$q(\alpha,t)$	power density	ΔN	the number of cycles for which the thermal behaviour is assumed not to change in the FE model
$\bar{Q}$	constant heat input rate	μ	coefficient of friction
$\bar{q}(\alpha)$	average power density		
q'	heat flux	ρ	density
R	Radius of the cylindrical specimen	ω	angular frequency of fretting

1. Introduction

Fretting is the small amplitude oscillation between two bodies in contact which occurs in a wide variety of mechanical systems. Although the amplitude of fretting is small (< 300 μm), fretting can cause serious damage including wear and fatigue [1]. It has been stated that over 50 parameters can influence behaviour in fretting [2]; amongst them, the temperature of the contact has been identified as having a significant influence on both the significance and mechanism of damage in fretting. This temperature is affected both by the environmental temperature and by the dissipation of frictional energy associated with the fretting motion itself. Since the total area of the asperity contacts is usually much smaller than the nominal contact area, the frictional heat dissipation at these points of contact will result in a high temperature being observed at these asperity tips; Blok [3] described this as the "flash temperature". In addition, Ashby et al. demonstrated that the mean surface temperature represents that "which would be reached if the frictional heat was injected uniformly across the nominal contact area, and is a good approximation to the temperature a few tens of microns below the actual surface" [4]. The flash temperature and mean surface temperature are not independent of each other, nor of the bulk temperature. The mean surface temperature is dependent upon the temperature of the heat sink (i.e. the bulk temperature), and in turn, the flash temperature is dependent upon the mean surface temperature [4].

The role of temperature in fretting has generally been attributed to changes associated with oxide debris formation and its development into a debris bed, and with changes in the properties of the material close to the surface [5]. Previous studies have suggested that the fretting wear rate of both carbon steel and stainless steel tends to fall rapidly once a certain critical ambient test temperature has been exceeded [6–9], with the change in behaviour being governed by oxide formation which is encouraged at elevated temperature [10]. Moreover, it has been demonstrated by a number of workers (e.g. Colombie et al. [11], Iwabuchi et al. [9]) that the rate and mechanism of wear is strongly dependent upon the formation of a stable oxide debris layer, and it has been argued that such a debris bed forms more readily as the temperature increases [10].

The dissipation of frictional power into the contact is dependent upon the applied load and the coefficient of friction (which between them control the tractional force), the slip amplitude and the frequency of oscillation. It is argued that it will be the density of frictional power dissipation (alongside the material properties) that will control the mean surface temperature, although it must be noted that in a traditional experimental fretting contact geometry (such as a cylinder-on-flat or sphere-on-flat), the mean power dissipation density is different for the curved and flat bodies within the pair. Of the three parameters which can be controlled in an experimental design, the fretting

frequency provides the clearest route to identifying the role of frictional power density dissipation (both the load and the slip amplitude affect other key parameters in the system, such as the area over which the power is dissipated). As the fretting frequency increases, the temperature within the contact will also increase, and it is argued that this will affect the debris formation and debris retention within the contact by mechanisms similar to those proposed when the role of ambient temperature has been considered. Indeed, a general reduction in wear rate has been found with increasing fretting frequency in previous studies [12–14].

It can be seen that both environmental bulk temperature and the frictional power dissipation (via the fretting frequency) have a critical influence on behaviour in fretting, and it is argued that these two parameters are not entirely independent, since both influence the temperature local to the contact (both the flash temperature and mean surface temperature). However, predictive techniques are required to facilitate study of the roles of these two parameters, since measurements of these temperatures are always difficult.

Jaeger [15] first gave a detailed analysis of the temperature rise in a semi-infinite body due to a moving heat source on top of the surface. He introduced the Péclet number into this problem to identify the relationship between the contact area, the heat input, the thermal properties of the material and the relative speed of the contacting bodies. Later, Archard [16] reduced the mathematical complexity of Jaeger's work and presented a simplified analysis of the temperatures in rubbing surfaces for both steady state (low speed sliding) and transient (high speed sliding) conditions. Tian and Kennedy [17] analysed the maximum and average flash temperatures in contacts associated with different shapes of heat source across a range of Péclet numbers, whilst Ashby et al [4] analysed the frictional heating problem via a particularly simple framework where they analysed the temperature in contact with two "equivalent linear-diffusion distances" for the two surfaces to the heat sink, and presented this analysis as a temperature map. The mathematical model for flash temperature presented by Ashby et al. made use of the relationship proposed by Greenwood and Williamson [18] between the real area of asperity contact, the applied load and hardness of the material.

Since fretting consists of small amplitude oscillation between two contacting bodies, the frictional power is dissipated over a relatively small area and thus the frictional heat input can be assumed to act as a continuous heat source. Indeed, it has been argued that the role of the motion of the contact in the dissipation of the frictional heat can be neglected because of the small displacement amplitude. For example, in considering fretting of a sphere-on-flat contact, Greenwood and Alliston-Greiner [19] assumed a sinusoidal heat input which was distributed uniformly over a circular contact area; they performed a general analysis of the steady state and periodic temperature in fretting by dividing the heat source via Fourier analysis, and demonstrated that a steady state mean temperature increase with a stable periodic variation was achieved relatively quickly. Attia and D'Silva [20] took a different approach and derived a dimensionless solution for the temperature rise in fretting by analysing a reciprocating moving heat source. The maximum flash temperature rise at the centre of the contact was predicted to be proportional to the frequency and amplitude of fretting. Similarly, Wen and Khonsari [5] presented a detailed analysis for various contact geometries with both uniform and parabolic heat input distributions on the surface, where they argued that the shape of the heat source had significant effects on the temperature distribution very close to the contact with a much smaller effect on the far-field temperature distribution [5]. The fact that the

real contact area between the asperities is much smaller than the nominal contact area results in a steep temperature gradient from the very top surface to the sub-surface layer in fretting [21,22]. Analytical models have developed to predict the flash temperature in fretting by Attia [22,23].

Whatever their basis and focus, these models are generally limited to the initial conditions within a fretting contact, but it is recognised that the temperature distribution will be influenced by the changes occurring during the wear process itself, since wear both alters the contact geometry, and results in the formation of a debris layer which may have very different thermal properties from those of the bulk materials being considered. Noting that the thermal conductivity of an oxide is typically about a tenth of that of the metal from which it is derived, Attia and D'Silva [20] concluded that the flash temperature rise developed with the inclusion of an oxide film in the contact can be two to six times greater than that developed in a clean (metal-to-metal) contact.

It has been argued that the mean temperature in the contact affects the manner in which the debris either forms into a stable bed or is ejected from the contact, and also the properties of the material close to the surface (which is exposed to the alternating stress fields associated with the fretting motion), but that the contact temperature will be influenced by changes which result from the fretting process itself, namely the formation of the debris layer and the geometrical changes. Unlike other methods, finite element modelling can be used to analyse the significance of these changes since it allows a time-marching approach to be employed. The aim of this work is to develop a finite element (FE) model to analyse the mean surface temperature in a wearing fretting contact for a cylinder-on-flat contact of steel and to validate the FE model via analytical models and experimental measurements. Such information will then provide a platform to better understand the role of the contact conditions on the dominant mechanisms controlling the fretting wear process; and it will provide any future FE modelling with the potential to apply temperature as an internal variable to better predict fretting wear.

2. Paper outline

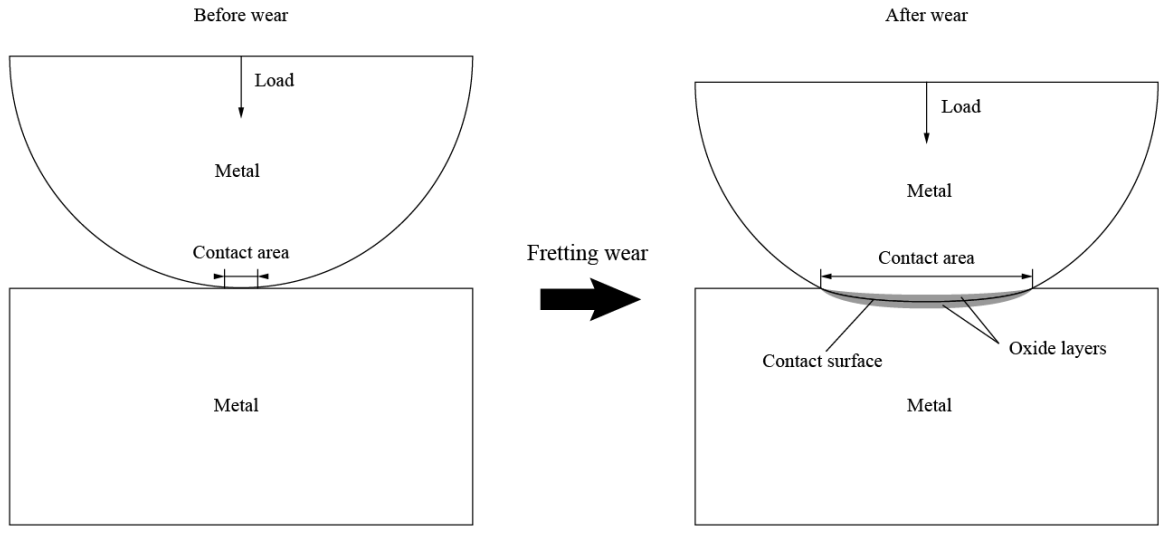

Figure 1 Illustration of the geometry changes and oxide debris layer formation induced by fretting wear

Previous work on the prediction of friction induced temperature rise in fretting contacts has mainly employed analytical models. However, as real surfaces are fretted against each other, there will be

two significant changes (as illustrated in Figure 1): (i) wear will result in geometrical changes, which will affect contact width and pressure distributions; (ii) debris layers will form on the worn surfaces, with these being primarily composed of oxides with thermal properties that are different from those of the substrate materials. These two factors are expected to have critical influence upon the local thermal field. However, analysis of such a problem is very complex to perform analytically, and accordingly, a numerical (finite element) technique has been employed in this context.

However, analytical models are still required in these endeavours: (i) the FE model itself needs benchmarking, and one method for this is to compare it with an analytical model; (ii) an analytical model is needed to set boundary conditions for the FE model to allow it to predict a long test for a semi-infinite space which is assumed in all models in this paper. However, any analytical models which have been used to benchmark the FE models also need to be validated themselves by benchmarking with each other and by comparing with experimental data as appropriate. In summary, experimental work, two analytical models and one FE model will be presented in this paper; their interactions (in terms of benchmarking (comparison between the models) and validation (testing the model by comparing with experimental measurements)) with each other are shown diagrammatically in Figure 2.

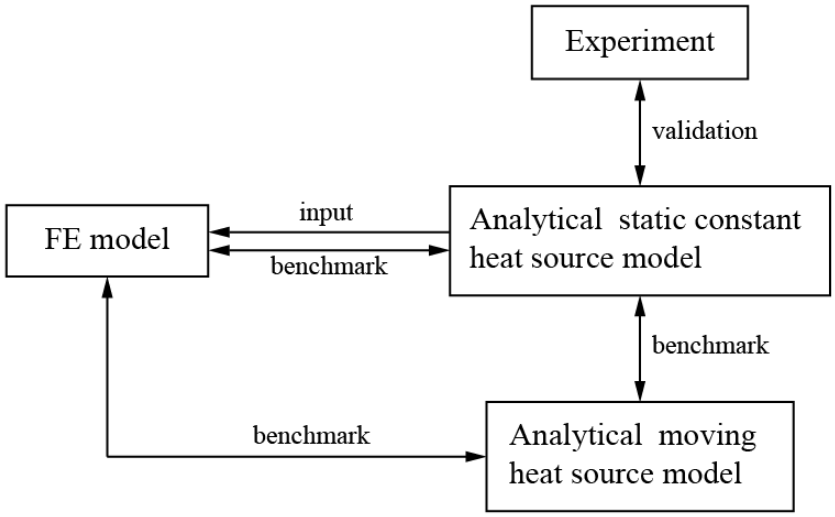

Figure 2 Interactions between the various models and experimental work described

2.1. Capabilities and limitations of the models

The capabilities and the limitations of the models which will be presented in this paper are summarised below to provide the reader with a coherent framework in which the models are presented. In all cases, the work here addresses the general temperature field, as opposed to the flash temperatures at the asperity tips. Throughout this work, references to the contact temperature refer to the mean surface temperature, rather than the flash temperature.

Analytical models:

1) ***Moving heat source model***

Summary description: The location and intensity of the power dissipated in a fretting contact varies since the contact point is moving. This model seeks to take these into account.

Capability: Able to predict the temperature variation in a contact throughout a fretting cycle (as a function of position and time).

Limitations: relatively high computational cost; cannot deal with more complicated conditions in fretting such as geometrical changes associated with wear and the formation of debris layers with different thermal properties. Due to its computational cost, this technique is limited to modelling behaviour over small number of fretting cycles.

2) ***Static constant heat source model***

Summary description: In this model, although the motion of the fretting contact controls the power dissipation, the motion itself is neglected in terms of the variations in power and position of power dissipation. As such, the model is based upon a constant (average) power dissipation at a fixed position.

Capability: Able to give good "far field" temperature prediction with very low computational cost which makes it suitable for modelling behaviour over extended number of fretting cycles.

Limitations: cannot predict the in-cycle temperature variation in the fretting contact; cannot deal with more complicated conditions in fretting such as geometrical changes associated with wear and the formation of oxide debris layers with different thermal properties.

FE model:

Summary description: a time-marching model, which addresses the effects of changes during the process (such as geometrical changes due to wear and the formation of oxide debris layers with different thermal properties).

Capability: Able to deal with more complicated and more realistic conditions which cannot be dealt with via the analytical models.

Limitations: highest computational cost. Due to its computational cost, cycle jumping is needed to model behaviour over large number of fretting cycles.

3. Experimental procedure

3.1. Specimen, test procedures and conditions

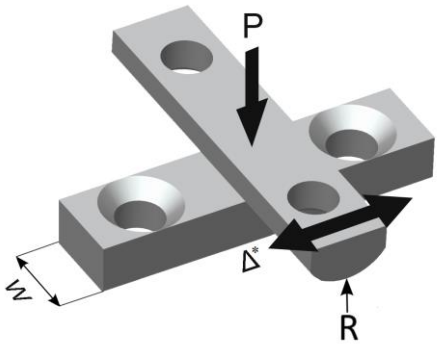

Figure 3 Cylinder-on-flat specimen arrangement in fretting test: *W* =10 mm, *R* = 6 mm, *P* = 450 N, and *Δ = 50 µm** [14]

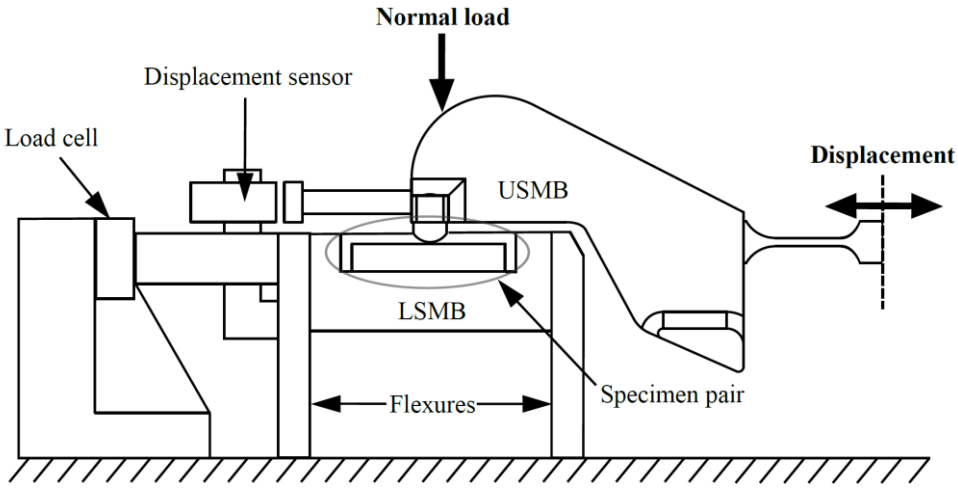

Figure 4 Main components of fretting apparatus [14]

Fretting experiments were conducted on 304 stainless steel specimens; the chemical composition of this steel measured by atomic emission spectroscopy (Foundry Master, Oxford Instruments, UK) is detailed in Table 1. The mechanical and thermal properties employed for the modelling of this material are presented Table 2. Specimens were assembled in a cylinder-on-flat arrangement (Figure 3) which generated a line contact of 10 mm in length and 114 µm in width (initial Hertzian contact width under the applied load in the experiment of 450 N). The flat specimen was mounted on the lower specimen mounting block (LSMB) which is stationary with the cylindrical specimen being mounted on the upper specimen mounting block (USMB). A normal load, P, was applied to the USMB through a dead-weight. The fretting motion was applied perpendicular to the axis of the cylindrical specimen through control of an electromagnetic vibrator (EMV). The far-field displacement of the USMB was measured through a capacitance displacement sensor which facilitated control of the relative displacement between the specimens. A piezoelectric load cell was used to measure the tangential force in the contact. Both the displacement and the tangential force were recorded continuously (200 samples per fretting cycle, independent of fretting frequency) and were plotted against each other as fretting loops; in addition, the maximum tractional force (Q^*) in each cycle was recorded. A schematic fretting loop (representative of those observed during the tests conducted) is presented in Figure 5, along with an example of a measured fretting loop. The slip amplitude (δ) represents the actual slip that occurs in the contact; it is measured from the fretting loops and is smaller than the applied displacement amplitude (Δ^*) due to compliances in the

contact and in the system more generally. To eliminate the commonly-observed effect of the variation in the tractional force across the fretting oscillation, the energy coefficient of friction calculated from the dissipated energy per cycle (E_d), was employed in the models as the coefficient of friction (μ) in this study [8]:

$$\mu = \frac{E_d}{4\,P\,\delta} \tag{18}$$

Table 1 Measured chemical composition of 304 stainless steel (wt%)

C	Si	Mn	P	S	Cr	Mo	Ni
0.027	0.816	1.79	0.013	0.025	17.2	0.303	10.3
Al	Co	Cu	Nb	Ti	V	W	Fe
0.003	0.083	0.347	0.012	0.008	0.044	0.035	Remainder

Table 2 Mechanical and thermal properties of 304 stainless steel, with superscripts referring to the relevant properties of the cylinder and flat respectively

E^f/E^c (GPa)	v^f/v^c	ρ (kg m^{-3})	k (W m^{-1} K^{-1})	C(J kg^{-1} K^{-1})
193	0.3	8030	16.2	500

(a) (b)

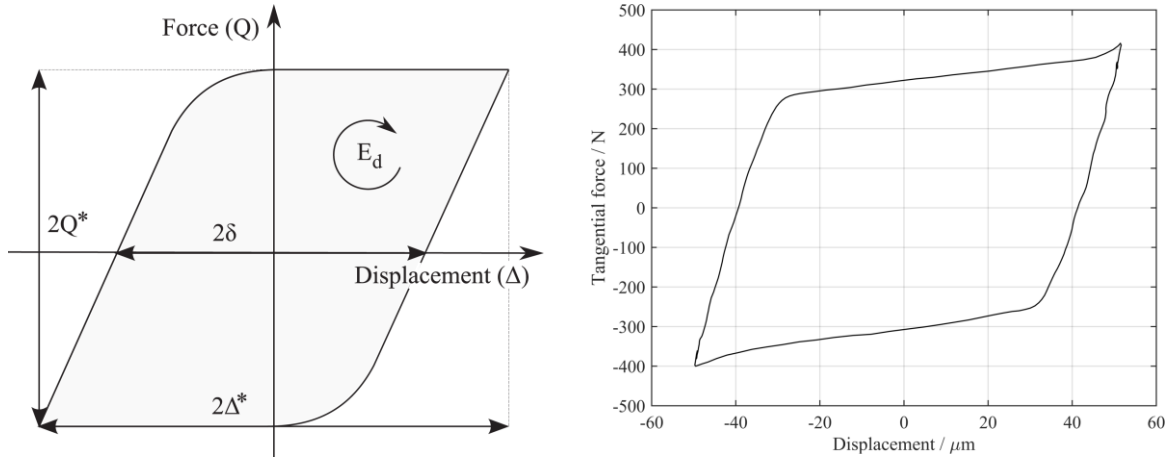

Figure 5 (a) Schematic fretting loop [10] **(b) Experimental fretting loop (15,000 cycles, P = 450 N, *f* = 20 Hz, Δ* = 50 μm)**

Tests were performed at normal laboratory temperatures (19 to 22 °C) at both a low fretting frequency (20 Hz) and a high fretting frequency (200 Hz). Test conditions are summarised in Table 2.

Table 3 Fretting test conditions

Normal load	*P* (N)	450
Applied displacement	*Δ** (μm)	50
Duration	*t* (s)	1000

Frequency	f (Hz)	20, 200
Temperature	T (°C)	Ambient

3.2. Temperature measurements associated with the fretting contact

The temperatures very close to the contact were measured via fine, sheathed thermocouples (Type K, TC Direct, UK). Holes of 0.3 mm diameter were drilled in the flat specimen, with the axis of the hole parallel to that of the line contact. The holes were drilled directly below the line contact at depths of 0.45 mm, 1.05 mm and 2.5 mm below the surface. Each hole was 5 mm in length such that when thermocouples were inserted, the thermocouple tip was at the centre of the 10 mm contact line. Sheathed thermocouples of 0.25 mm diameter were inserted into the holes. As the drilling of the hole will remove part of the specimen material, it is recognised that its presence may influence the temperature distribution around the holes. To minimise this influence, the holes 0.45 mm and 2.5 mm beneath the surface were drilled from one side of the specimen whilst the hole 1.05 mm beneath the surface was drilled from the other side of the specimen.

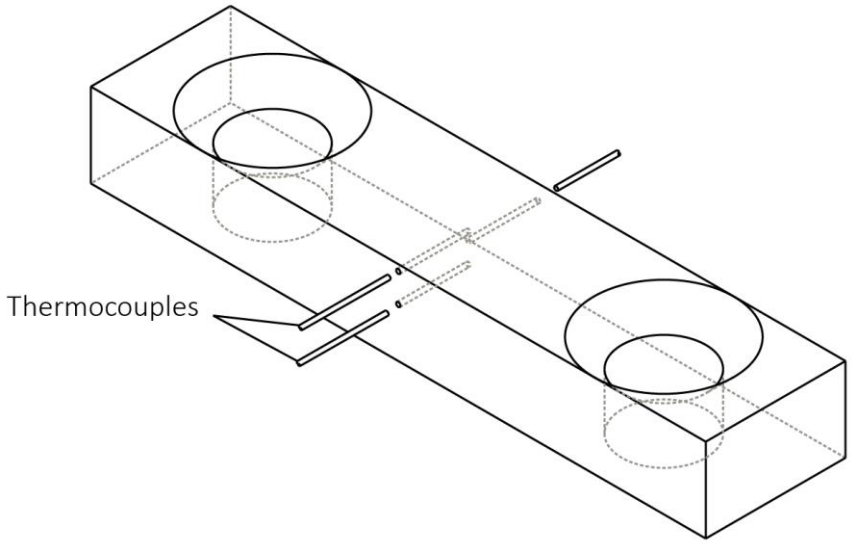

Figure 6 Illustration of the positions of the thermocouples within the flat fretting specimen

4. Development, benchmark and validation of the models

4.1. Development of analytical models

Whilst there are limitations to analytical models when studying the contact temperature in fretting (e.g. the inability to take into account changes in contact geometry due to wear, the inability to account for oxide retention in the wear scar etc), they do provide a means by which numerical models can be benchmarked before they are applied to more complex (and thus more realistic) situations. In this work, analytical models were based on the initial contact conditions (including geometry). Methods used in previously reported studies [5,20] were applied to the cylinder-on-flat fretting contact with the geometry being derived by application of a Hertzian contact model.

4.1.1. Moving heat source model

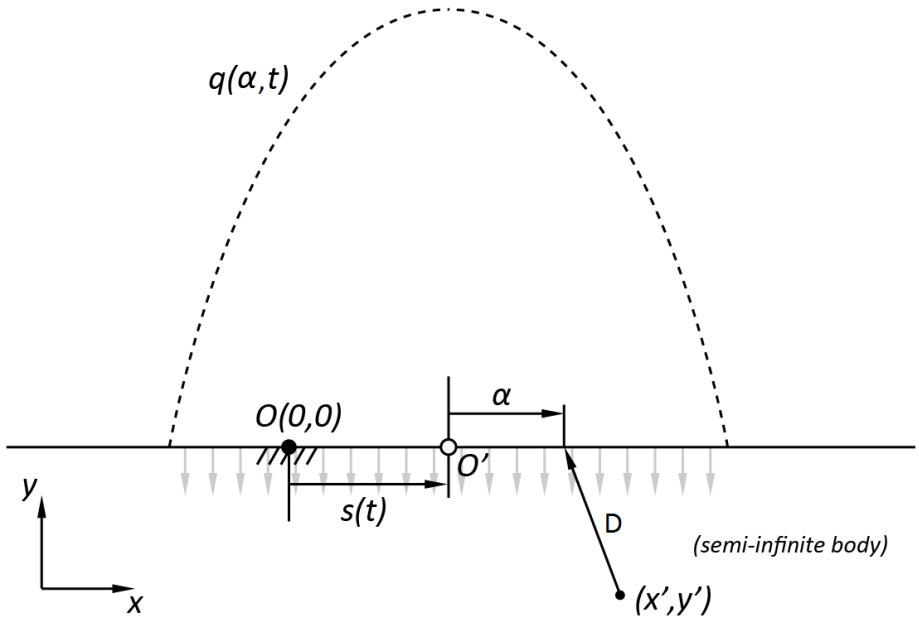

Figure 7 Moving heat source on a semi-infinite body: *O* is the fixed origin which is the centre of the initial contact area on the flat; *O'* is the moving origin which is the centre of the slider; the dashed line represents the power of the heat input *q(α, t)* which is proportional to the contact pressure.

The temperature rise in the fretting contact is assumed to be caused by the dissipation of frictional power only and all of the frictional work dissipated was assumed to be converted into heat. The two contacting bodies are set to have same material properties and the frictional energy dissipated is assumed to be partitioned equally into the two bodies. The overall power of the heat source *Q(t)* is given as:

$$Q(t) = F_f \cdot |v(t)| = P \cdot \mu \cdot |v(t)| \tag{1}$$

where F_f is the frictional force, P is the applied normal load, μ is the coefficient of friction and $v(t)$ is the sliding velocity.

Fretting operates under small amplitude oscillation around an origin. To simulate the behaviour of such motion, the slider is assumed to have sinusoidal motion related to the fixed origin *O* (0, 0) which is the centre of the initial contact area on the flat. *O'* is defined as the centre of the moving body (i.e. the origin of this latter body); accordingly, the position of the moving origin *O'* as a function of time (*s(t)*) can be represented as:

$$s(t) = \delta \cdot \sin(\omega t) \tag{2}$$

where $\omega = 2\pi \cdot f$, and f is the frequency of fretting. The corresponding velocity, $v(t)$, of the slider is given by the following equation:

$$v(t) = \frac{ds}{dt} = \delta \cdot \ \omega \cos(\omega t) \tag{3}$$

Therefore, the overall power of the heat source ($Q(t)$) can be defined as a function of time:

$$Q(t) = F_f \cdot |v(t)| = P \cdot \mu \cdot \delta \ \cdot \omega \cdot |\cos(\omega t)| \tag{4}$$

The cylinder-on-flat arrangement is assumed to produce a uniform line contact, and conduction is considered to be the major term of heat dissipation in the fretting wear process (the heat loss due to convection and radiation from the surfaces is neglected). Accordingly, the problem can be simplified as a line heat source on a semi-infinite body, and thus treated as a two-dimensional problem. The contact will deform elastically under load, and thus the heat is dissipated over the area of the contact rather than over a line. The coefficient of friction is assumed to be constant across the contact (i.e. independent of contact pressure), and therefore, the power density is proportional to the contact pressure at any point within the contact. The contact pressure distribution (*p(α)*) for a cylinder-on-flat contact is a function of the distance (*α*) from the centre of the heat source (see Figure 5), which can be calculated according to the Hertz elastic contact model as follows [24]:

$$p(\alpha) = p_0 \sqrt{1 - \frac{\alpha^2}{b^2}} \quad (-b \le \alpha \le b) \tag{5}$$

where p_0 is the maximum contact pressure which appears at the centre of the contact area and *b* is the elastic half-width of the contact. In turn, expressions for these parameters are as follows:

$$p_0 = \left(\frac{P'\,E^*}{\pi\,R}\right)^{1/2}, \quad b = \left(\frac{4\,P'R}{\pi\,E^*}\right)^{1/2} \tag{6}$$

where *P'* is the normal load per unit length applied across the contact, *E** is the composite modulus of the two contacting bodies and for a cylinder-on-flat contact, *R* is the radius of the cylinder. Under the plane strain conditions:

$$E^* = \left(\frac{1 - \left(v^f\right)^2}{E^f} + \frac{1 - (v^c)^2}{E^c}\right)^{-1} \tag{7}$$

where E^f and E^c are the Young's moduli of the flat and cylindrical specimens respectively and v^f and v^c are their respective Poisson's ratios.

Therefore, the power density as a function of position and time, $q(\alpha, t)$, can be expressed as:

$$q(\alpha, t) = p(\alpha) \cdot \mu \cdot \delta \cdot \omega \cdot |\cos(\omega t)| \tag{8}$$

The solution of the temperature rise (δT) resulting from an instantaneous line heat source in an infinite space has been given by Carslaw and Jaeger [25]:

$$\delta T = \frac{q(\alpha, t)}{4\pi\,\kappa\,t} e^{-\frac{D(\alpha,t)^2}{4\,\kappa\,t}} \tag{9}$$

where $\kappa = \frac{k}{\rho\,C}$, in which *k* is the thermal conductivity, *ρ* is the density, and *C* is the specific heat capacity of the material in question. $D(\alpha, t)$ is the distance from a chosen point within the contact (i.e. a point heat source) to a defined point in the body (*x', y'*), at time *t*, which can be represented as follows based on the function of the slider's displacement (Figure 7):

$$D(\alpha, t) = \sqrt{\left(x' - \left(\alpha + s(t)\right)\right)^2 + y'^2} \tag{10}$$

The temperature rise (ΔT) at the defined point (x', y') at a time t' can be calculated by integrating the instantaneous temperature rise solution across the whole contact area (i.e. integrating the effects of the individual point sources) and over the time period since the motion began:

$$\Delta T = \int_{t=\,o}^{t'} \int_{\alpha=\,-b}^{b} \delta T \; d\alpha \; dt$$

$$\Delta T = \int_{t=\,0}^{t'} \int_{\alpha=\,-b}^{b} \frac{q(\alpha, t)}{4\pi\kappa(t' - t)} e^{-D(\alpha,t)^2/4\kappa(t'-t)} d\alpha \; dt \tag{11}$$

Numerical integration is used to solve equation 11. The contact area (from $\alpha = -b$ to b), which is also the area of the heat source, is discretised into m increments with a step length of $\Delta\alpha$. And the whole time period (from $t = 0$ to t') is discretised into n increments with a step length of Δt. Therefore, the total temperature rise can be calculated as:

$$\Delta T = \sum_{j=0}^{n} \sum_{i=0}^{m} \frac{q\left(\alpha_{i,j}, t_{i,j}\right)}{4\pi\kappa\left(t' - t_{i,j}\right)} e^{-D\left(\alpha_{i,j}, t_{i,j}\right)^2/4\kappa\left(t'-t_{i,j}\right)} \Delta\alpha \; \Delta t \tag{12}$$

The results presented in this work have been derived with $\Delta\alpha = 0.114 \; \mu m$ and $\Delta t = 0.23 \; \mu s$.

4.1.2. Static constant heat source model

The model described in section 4.1.1 treated the fretting frictional heat source as a sinusoidally moving heat source and seeks to predict the variation of the local temperature due to the variations in both position and power dissipated. However, the numerical double integration is time consuming (computationally resource intensive) when very large numbers of fretting cycles are involved. Under fretting conditions, the slider performs a reciprocating motion with displacement amplitudes which are generally small compared to the distances over which the heat diffuses over the time period of the test. Accordingly, when considering the temperature rise over the period of the test, a simplification can be made where the fretting heat source is treated as a static one. Greenwood and Alliston-Greiner [19] considered a static heat source with either a constant (average) power input or with a sinusoidally varying power input (see equation 4), and demonstrated that the difference in the temperature rise at the contact between the two cases was less than 7%. Accordingly, as well as assuming the contact to be static, when predicting the overall local temperature rise, it is reasonable to consider the situation being adequately represented by a constant heat input rate (power), $\bar{Q}$, as follows:

$$\bar{Q} = P \cdot 4\delta \cdot \mu \cdot f \tag{13}$$

Therefore, the power density (heat input per unit time per unit area) ($\bar{q}(\alpha)$) can be expressed as:

$$\bar{q}(\alpha) = p(\alpha) \cdot 4\delta \cdot \mu \cdot f \tag{14}$$

According Carslaw and Jaeger [25], the solution of the temperature rise ($\delta\bar{T}$) of an infinitely long constant line source on a semi-infinite body is given by:

$$\delta\bar{T} = \frac{\bar{q}(\alpha)}{4\pi \; k} \left(ln \frac{4kt}{D(\alpha)^2 \rho C} - \gamma\right) \tag{15}$$

(where the Euler constant, γ, = 0.5772…). $D(\alpha)$ can be calculated as:

$$D(\alpha) = \sqrt{\left(x' - \alpha\right)^2 + y'^2} \tag{16}$$

Thus, the temperature rise ($\Delta\bar{T}$) at a point (*x′, y′*) in the semi-infinite body can be calculated as:

$$\Delta\bar{T} = \int_{-b}^{b} \delta\bar{T}\, d\alpha$$

$$\Delta\bar{T} = \int_{-b}^{b} \frac{\bar{q}(\alpha)}{4\pi\, k} \left(ln \frac{4kt}{D(\alpha)^2 \rho C} - \gamma\right) d\alpha \tag{17}$$

4.2. Benchmarking of the analytical models against each other and validation of the analytical models against the experimental measurements

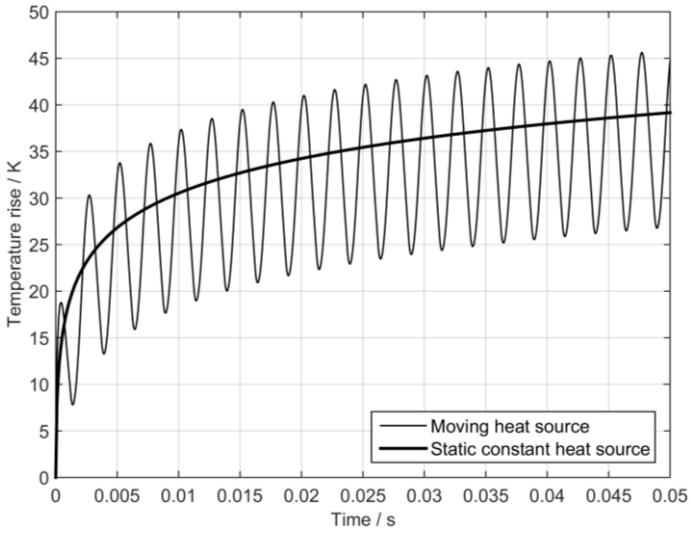

Figure 8 Prediction of temperature rise at the fixed origin from the analytical models in the first ten cycles (*P* = 450 N, *f* = 200 Hz, δ = 50 µm, μ = 0.61)

Figure 8 shows the evolution of surface temperature rise (above the starting temperature) with time obtained from the analytical moving heat source model for the first ten cycles of fretting at a frequency of 200 Hz. The slip amplitude is assumed to be equal to the displacement amplitude in such prediction and an averaged coefficient of friction (μ) of 0.61 (derived from the fretting testing) has been applied. It can be seen that a sinusoidal variation in temperature (at twice the frequency of the fretting frequency, due to the contact passing the fixed origin twice per fretting cycle) with an amplitude of ~ 9 K is superimposed upon a more gradual increase in the mean temperature. It can also be seen from Figure 8 that the mean temperature increased significantly in a very short time (~ 35 K temperature rise in the first ten cycles with a time duration of 0.05 s); however, the rate of increase decreased rapidly with time. The solution from the static constant heat source model generally follows the same trend of the temperature rise from the simplified moving heat source model. However, the cyclic variation cannot be predicted in the static constant heat source model; moreover, the temperature rise is about 1 K higher than the average value from the moving heat source model for the conditions examined.

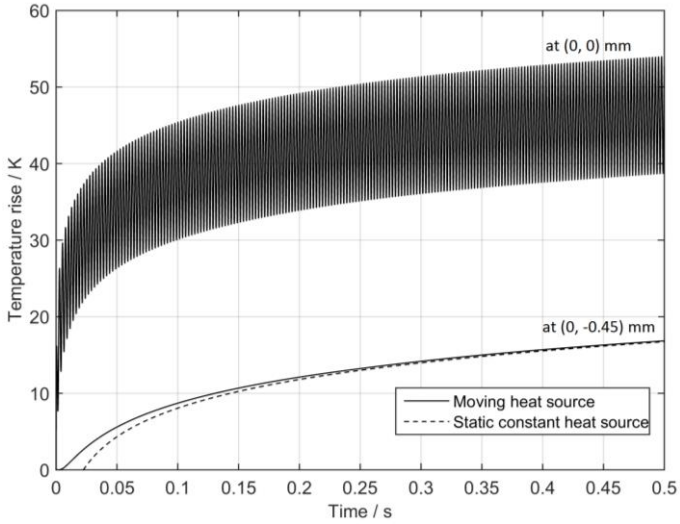

Figure 9 Comparison of temperature rise at fixed origin *O* (0, 0) and (0, - 0.45) mm for the first 100 cycles (*P* = 450 N, *f* = 200 Hz, δ = 50 µm, μ = 0.61)

The moving heat source model was used to predict the temperature rise both at the fixed origin (0, 0) and just below the surface at (0, -0.45) mm, with the latter being the position of the thermocouple closest to the surface in the experimental work; the results are shown in Figure 9. It can be seen that at O (0, 0), the variation of the temperature within a single cycle increased and became almost constant at about 15 K after about 0.1 second. However, at the subsurface measurement point (0, -0.45) mm, almost no variation in temperature on the timescale of the fretting cycles was observed, with instead a general increase in the predicted temperature rise with time. The evolution of temperature at this subsurface position (using the moving heat source model) gives a good comparison with the solution from the static constant heat source model especially after 0.2 s. It indicates that the much less computationally expensive static constant heat source model is preferred over the moving heat source model for thermal field predictions at this distance (and greater) from the contact. In terms of the predictions from these models, it is also notable that the mean temperature rise is around 30 K higher at the point (0, 0) mm than it is at (0, - 0.45) mm after 0.5 s for the modelling conditions selected.

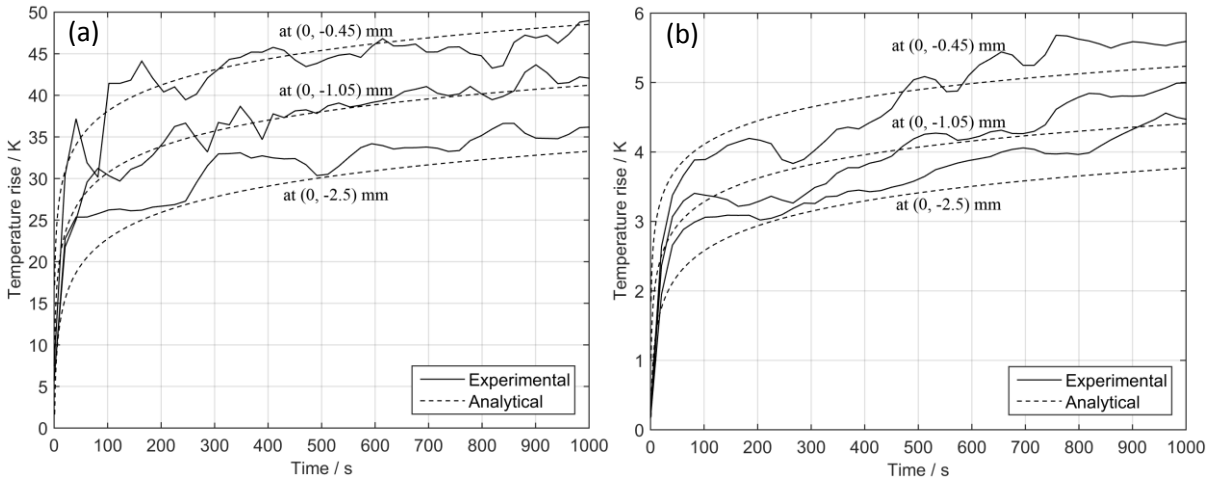

Figure 10 Comparison of measured temperature rise and results calculated by the analytical model with the static constant heat source for three positions, *x* = 0 mm, and *y* = - 0.45, - 1.05 and - 2.5 mm (*P* = 450 N, *Δ = 50 µm); (a) *f* = 200 Hz (b) *f* = 20 Hz. For context, it is noted that the initial contact semi width is 57 µm.**

Figure 10 shows the experimentally measured temperature rise over 1000 s for fretting at both 200 Hz and 20 Hz at the contact centre (x = 0) from thermocouples at three depths below the surface (y = -0.45, -1.05 and -2.5 mm). The corresponding predicted evolution of temperature (from the analytical static constant heat source model) for each of the positions is presented alongside. It can be seen that (for times longer than 100 s), the differences between the measured and predicted results are no more than 15% for all three positions and for both of the fretting frequencies examined, despite experimental fluctuations in temperature being observed. As discussed previously, the model assumes an isotropic material which exhibits constant thermal properties throughout the test duration and that the geometry of the contact does not change from the initial conditions. In reality, the thermal properties of the contact may change during the fretting process due to changes in contact geometry due to wear and the build-up of a debris layer. "The formation of debris layers on the two specimens may not proceed evenly, which will result in uneven partition of the heat energy into the two specimens; this would account for the short-term variations in temperatures observed. However, despite these simplifications, the correlation between the model and experimental observations is reasonable, which indicates that these simplifications have some validity.

4.3. Development of the FE model

A finite element (FE) based model has been developed to simulate the temperature rise in a fretting contact using the Abaqus FE code. A uniform line contact is employed for the cylinder-on-flat arrangement; for simplification, the contact is assumed to be infinitely long, with the model thus becoming a two-dimensional problem. Accordingly, two-dimensional coupled temperature-displacement plane strain elements were employed.

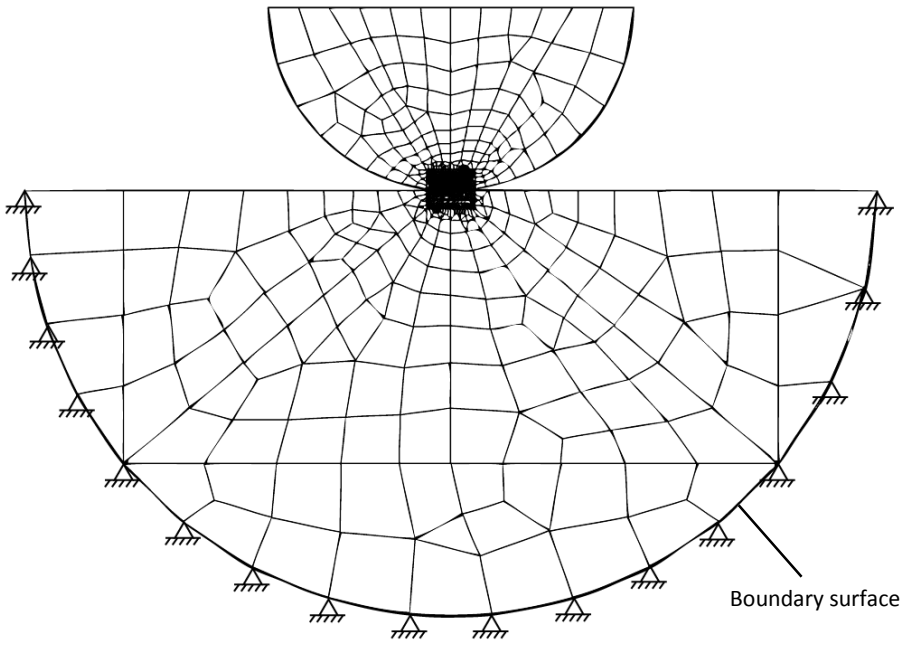

Figure 11 FE model for fretting test simulation

Figure 11 shows part of the overall geometry and the arrangement of the model. To model the cylinder-on-flat contact, the upper part is composed of a semicircle of 6 mm radius, and this is placed in contact with a lower specimen with a flat surface. A constant static vertical load and a

sinusoidal horizontal displacement were applied to the top line of the upper part. The bottom of the lower part is constrained as indicated in Figure 11.

In the contact zone, an extremely fine mesh (around 10 μm in dimension) was generated in order to capture the contact behaviour. The heat source was based on the assumption that all the work done overcoming friction is dissipated in the form of heat. The heat flows into the contacting bodies from the contact area and the local power density is deemed to be proportional to the local contact pressure. As the heat source only affects a small area, the temperatures for both bodies are expected to be similar; therefore, the thermal energy was assumed to partition equally into the two bodies.

Similarly to the analytical model, the majority of heat transfer is due to conduction into the bodies (the heat loss due to convection and radiation on the surfaces is again neglected). To model the bodies as "semi-infinite", the lower part needs to be large; which may significantly increase the computational cost. However, it has been found that for this system (and over the timescales of interest), the heat is conducted into the "semi-infinite" body over a relatively small area, which can be viewed as a line source (a point in the 2-D model). In addition, the material is assumed to have isotropic thermal properties; as such, a semi-circular shape can be employed for the lower part, as it provides equal conduction length for heat flows in each direction, which makes most efficient use of the elements. Moreover, when simulating the thermal behaviour in a fretting test over a longer duration, a surface condition can be set on the boundary surface (Figure 11) which will result in a heat flow (which is only a function of time) out of the specimen (perpendicular to that surface). The corresponding heat flux (*q'*) at the boundary surface as a function of time is calculated by the static constant analytical model at the bottom of the curved surface:

$$q' = -k\frac{d\Delta\bar{T}}{dD} \tag{19}$$

As such, this will allow long term simulations be performed at relative small computational cost.

Fretting tests usually consist of large numbers of cycles (often > 10^5 cycles). To simulate the temperature rise throughout the fretting test, computational optimization was operated with the assumption that the heat transfer behaviour is constant for a certain number of cycles. The conduction equation for this can be written as:

$$\Delta N \cdot \frac{\partial T}{\partial t} \cdot \rho c = \Delta N \cdot \frac{\partial}{\partial x}\left(K\frac{\partial T}{\partial x}\right) + \Delta N \cdot q \tag{20}$$

where ΔN is the number of cycles for which the thermal behaviour is assumed not to change. Therefore, computational optimization can be achieved by simply multiplying the heat input and the thermal conduction by ΔN. With this method, the temperature rise for N cycles of fretting can be predicted in $N / \Delta N$ increments of the simulation. It should be noted that cyclic temperature variation is not predictable if the cycle jump described above is applied. Therefore, the movement of the upper part is applied with constant speed in this case to allow the average temperature rise to be predicted.

4.4. Benchmarking of the FE model against the analytical models

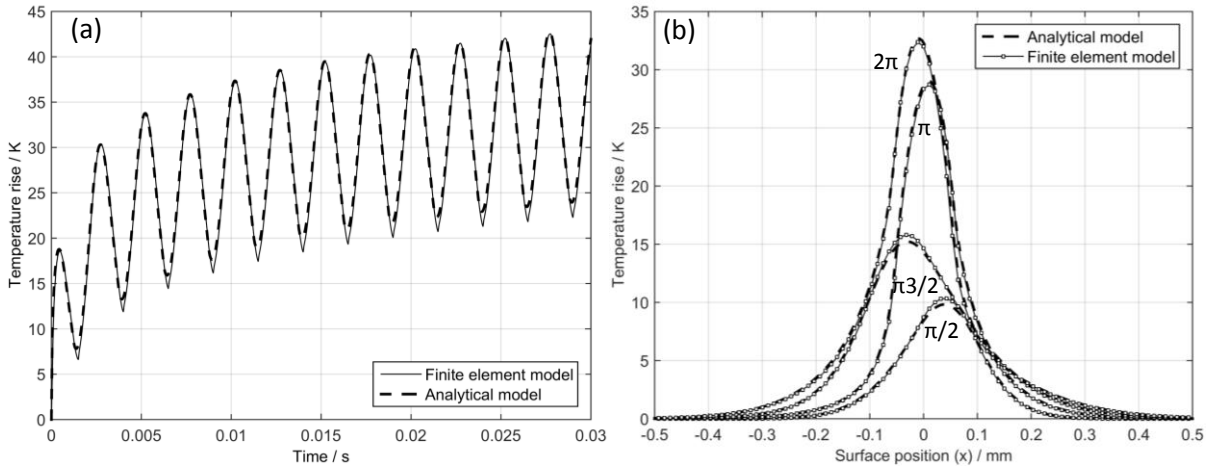

Figure 12 Comparison of analytical and FE predictions of temperature rise caused by a sinusoidal moving heat source (a) at the fixed origin in the first 0.03 s (b) on the top of the surface at the four phases in the first cycle (*P* = 450 N, *f* = 200 Hz, δ = 50 µm, μ = 0.61)

Figure 12 shows the comparison of the analytical moving heat source model and the finite element model in temperature rise prediction with a sinusoidally moving heat source. Comparisons have been made (a) at the fixed origin for the first 0.03 s and (b) along the contact surface for four phases in the first cycle. Good agreement is observed for both comparisons between the two models. Therefore, the ability of the FE model to replicate the analytical results in this simple case can be confirmed.

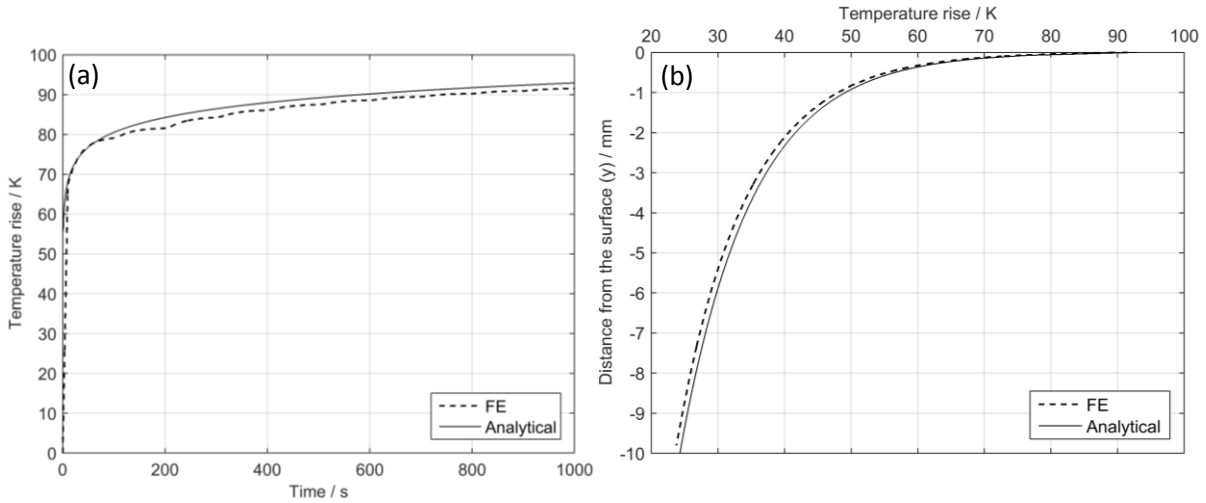

Figure 13 Comparison of analytical (static constant heat source) and FE predictions of temperature rise (a) at the fixed origin over a period of 1000 s (b) along the centreline (x = 0) as a function of distance below the surface at 1000 s (*P* = 450 N, *f* = 200 Hz, δ = 50 µm, μ = 0.61)

Figure 13 shows the comparison of the analytical constant static heat source model solution and the FE solution (a) at the fixed origin in large number of cycles (200,000 cycles) and (b) along the centreline (x = 0) as a function of distance below the surface at 1000 s. The FE model in this case was performed with a cycle jump of ΔN = 4000 (the accuracy of the selected cycle jump has been validated by good comparison with the results from simulations with smaller cycle jumps under small numbers of cycles); and it has the static constant analytical model as an input to set the boundary condition as outlined in the previous section. It can be seen that the FE solution gives a constant under-prediction of about 1 K (less than 2% of the overall temperature rise) compared to

the analytical solution for times greater than 100 s at the fixed origin. Good agreements have also been observed along the centreline below the surface at 1000 s; the difference is also about 1K between the prediction temperature rises between the two models. This demonstrates that the FE model with the computational optimizations produced very close results to the validated analytical model (static constant heat source) for the whole thermal field when the model is being used to predict the temperature rise long duration tests.

4.5. Disruption of the experimental thermal field by the presence of the thermocouples

In the experimental work conducted to examine the thermal fields, holes have been drilled to accommodate the thermocouples just below the contact. Considering the small size of heat source, the effect of these holes on the development of the thermal field needs to be considered; the significance of this influence can be analysed by FE modelling. In reality, heat transfer across the hole boundary will still occur as the thermocouple is positioned in the hole; however, due to the air gap and the lower thermal conductivity of the thermocouple, a significant reduction in thermal conductivity for the hole area is expected. In this study, the most extreme condition will be considered by applying a thermal conductivity of zero for the holes within the FE mesh (see Figure 14).

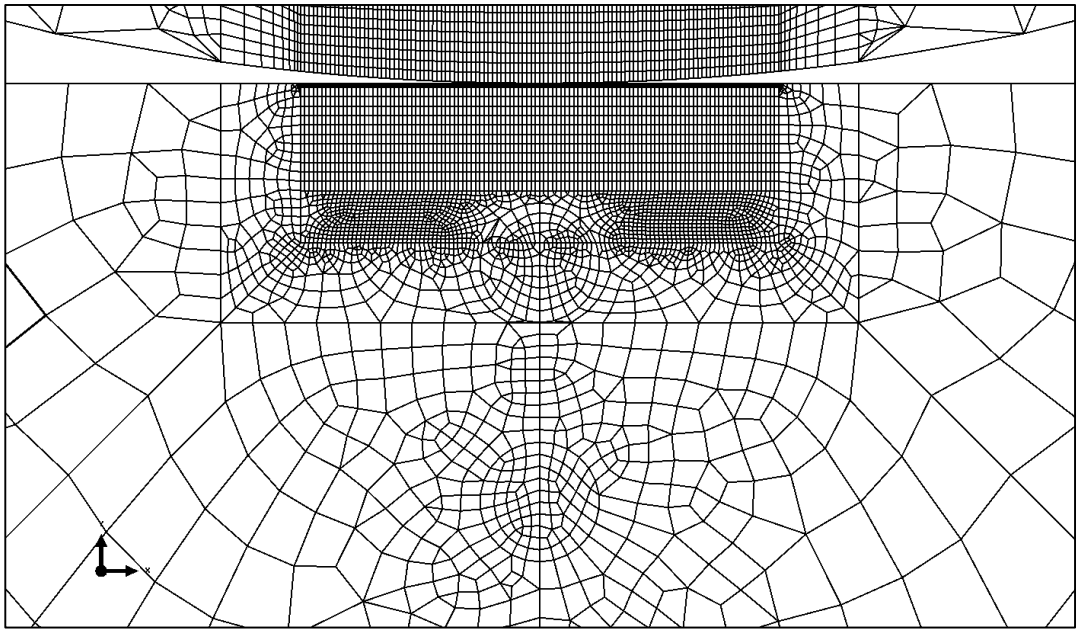

Figure 14 FE model with the inclusion of the thermocouple holes below the contact indicated

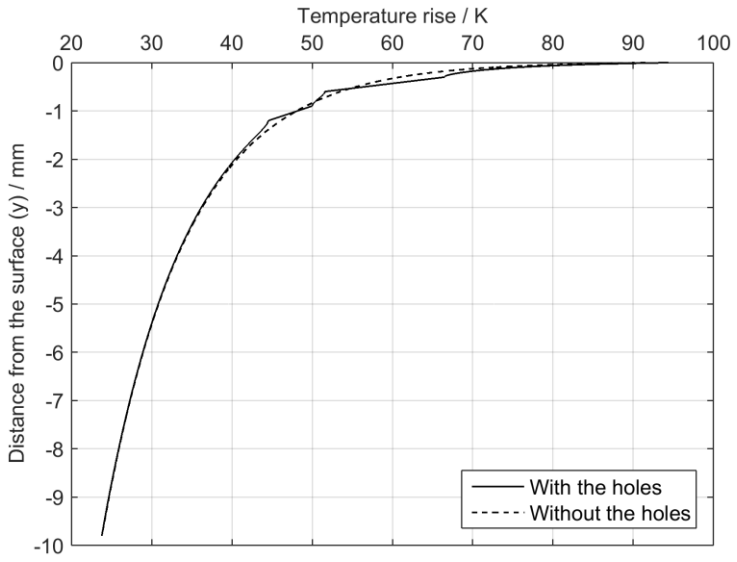

Figure 15 Comparison of the predicted centreline (x = 0) temperature rise as a function of distance below the surface from the FE model with and without the drilled holes (P = 450 N, f = 200 Hz, δ = 50 µm, μ = 0.61, t = 1000 s)

The temperature distribution predicted from the FE model with and without the thermocouple holes has been compared with each other on the contact centre-line (x = 0) at a range of depths below the surface (y being varied between 0 mm and -10 mm (Figure 15)). It can be seen that there are obvious temperature differences between the two models in the regions close to the holes themselves; however, the temperature rise near the contact and at depths below the holes are almost identical in the two models. This indicates that the temperature outside the hole will not be significantly influenced by the presence of the holes, and therefore, the existence of the holes themselves will not lead to a significant inaccuracy in temperature measurement.

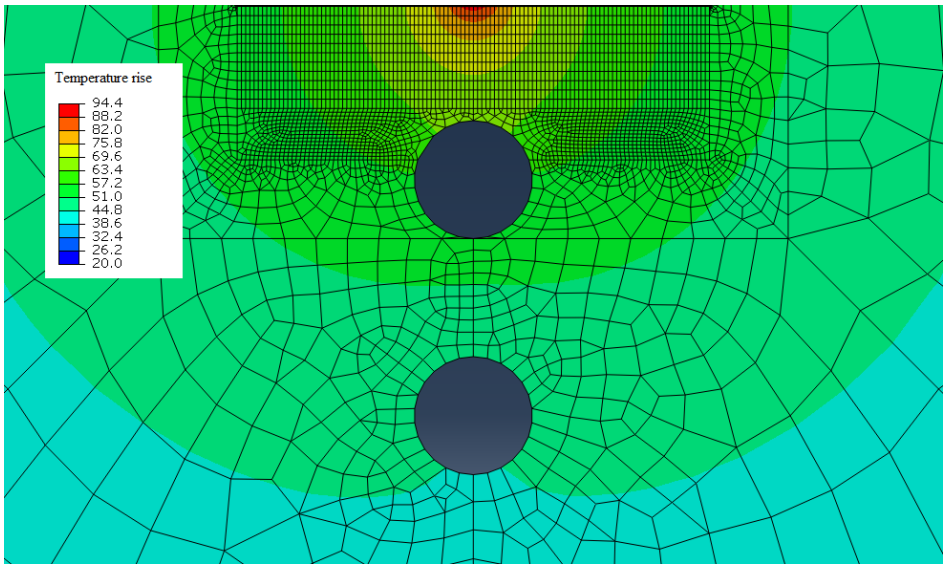

Figure 16 Contour of the temperature distribution around the holes 0.45 mm and 1.05 mm below the origin (P = 450 N, f = 200 Hz, δ = 50 µm, μ = 0.61, t = 1000 s)

Figure 16 shows the contours of the temperature distribution around the holes. Discontinuities can be observed around the holes (in particular, around the hole closer to the surface). The presence of the holes raised the temperatures in regions above the holes (i.e. in regions closer to source of heat

in the contact itself) and reduced the temperatures further away from the contact. This observation is in broad accord with the conclusion of previous work [26] which conducted detailed analysis on the effect of the thermocouple on the surrounding thermal field, making use of a much more complex 3D model. The model presented here indicates that the overall influence of the thermocouple holes upon the thermal field is small; given the other simplifying assumptions made in this model, it is argued that it is not inappropriate to ignore the distorting effects of the thermocouples on the thermal field.

5. Demonstration of the effects of geometry changes and oxide debris layer via application of the FE model

5.1. Development of more complex FE models

5.1.1. Inclusion of geometry changes

As outlined previously, the analytical models cannot take into account changes in the contact geometry during the test due to wear (the prediction of the temperature in contact is based on the initial contact conditions). However, with the FE model, fretting wear can be simulated and its effects on the development of the thermal field can be predicted. The FE-based fretting wear model first developed by McColl et al. [27] was applied to simulate the development of the wear scar. This methodology modified the Archard equation to calculate the incremental wear depth, dh, based the local contact pressure *p(α)* and the incremental local slip distance, *dS*, which can be presented by the equation below:

$$dh = A \cdot p(\alpha) \cdot dS \tag{21}$$

where *A* is the wear coefficient. In this work, wear coefficients of $2.5 \times 10^{-8}\ \mathrm{MPa}^{-1}$ (200 Hz) and $4 \times 10^{-8}\ \mathrm{MPa}^{-1}$ (20 Hz) were employed, based upon data presented by the authors in a previous paper [28] which explored the behaviour of the same material under similar test conditions.

5.1.2. Inclusion of the oxide layer

During the process of a fretting wear test, in addition to geometrical changes, oxide debris may be formed and retained in the contact, with the oxide-based debris layer being believed to form at a relatively early stage of the fretting process [29]. Therefore, for most of the time, the fretting contact is not between two metallic bodies, but is actually between two metallic bodies with a debris layer in between them. The thickness of the debris layer on each of the bodies is normally less than 10 μm. However, as the thermal conductivity of an oxide is generally lower than that of the bulk material, the thin debris layer can hinder the conduction of heat away from the moving contact (where it is generated) and, therefore, lead to an additional increase in the temperature of the contact itself. Moreover, the temperature of the debris layer will influence the stability of the debris layer itself [10] and the properties of the bulk material near the contact, which may strongly influence the subsequent wear behaviour. To study the effect of the debris layer on the thermal field, thin layers of elements were generated on the top surface of the flat specimen with these elements being assigned thermal properties which represent those of an oxide layer. The mechanical properties of the oxide debris layer also differ from those of the main bodies and can cause different pressure distribution in the contact. Everitt et al. [30] measured the Young's modulus of the debris layer formed during fretting of a titanium alloy, and found that the Young's modulus of

the debris layer was about 10% lower than that of the bulk material. However, due to its very low thickness, the influence of this difference in properties on the thermal field is expected to be small. This has been validated by assigning an appropriately reduced Young's modulus to the oxide-based debris material and comparing this to the case where the mechanical properties of the debris layer were assumed to be the same as those of the bulk material; it was shown that the difference in temperature rise between these two cases was always much less than 1%. In light of this lack of sensitivity, and the fact that the mechanical properties of these complex oxide-based debris layers are not always known, the mechanical properties of the oxide layer have been assumed to be the same as those of the bulk material.

The thermal properties employed for modelling of the oxide debris layer were obtained from the general literature relating to iron oxides since no experimental data were available which related to the thermal properties of a fretting-derived debris layer. However, across the literature surveyed, there were differences in the iron oxide types being considered, and differences in test methods, and accordingly, the measured thermal properties varied widely. The main constituent of oxide in a low temperature (below 200 °C) fretting contact is expected to be haematite (Fe_2O_3) [7]; at the same time, the oxide particles are expected to be compacted together because of the high contact pressure experienced in a fretting contact. Therefore, the literature survey has focussed on studies which have reported on the thermal properties of compacted haematite specimens. These studies suggested that the density of compacted haematite is around 5000 kg m^{-3} and that the specific heat capacity is around 1000 J $kg^{-1}{\cdot}K^{-1}$ [31,32] and accordingly, these values have been utilised in the FE study. However, the thermal conductivity reported varies widely across different studies (Table 4) from between 0.44 W m^{-1} K^{-1} to 6.4 W m^{-1} K^{-1}. Accordingly, in the current FE study, two thermal conductivities broadly spanning this range (1 W m^{-1} K^{-1} and 5 W m^{-1} K^{-1}) have been utilised to examine the influence of this parameter on the predicted evolution of the thermal field (these values cover the ratio of the thermal conductivities of the oxide and metal of 0.1 as suggested by Attia and D'Silva [20]). The FE model was developed to examine the effect of presence of the oxide-based debris layer in the development of the thermal field, with debris layer thicknesses between 2 µm and 10 µm (in line with observations reported in the work of Pearson et al. [10]).

Table 4 Thermal conductivities of haematite reported in the literature

	Shinde and Rajpure [33]	Torres and Colas [32]	Endo et al [34]	Molgaard and Smeltzer [35]
k (W m^{-1} K^{-1})	0.44	1.2	3.8	6.4

5.2. Results

5.2.1. Effects of geometry changes

(a)

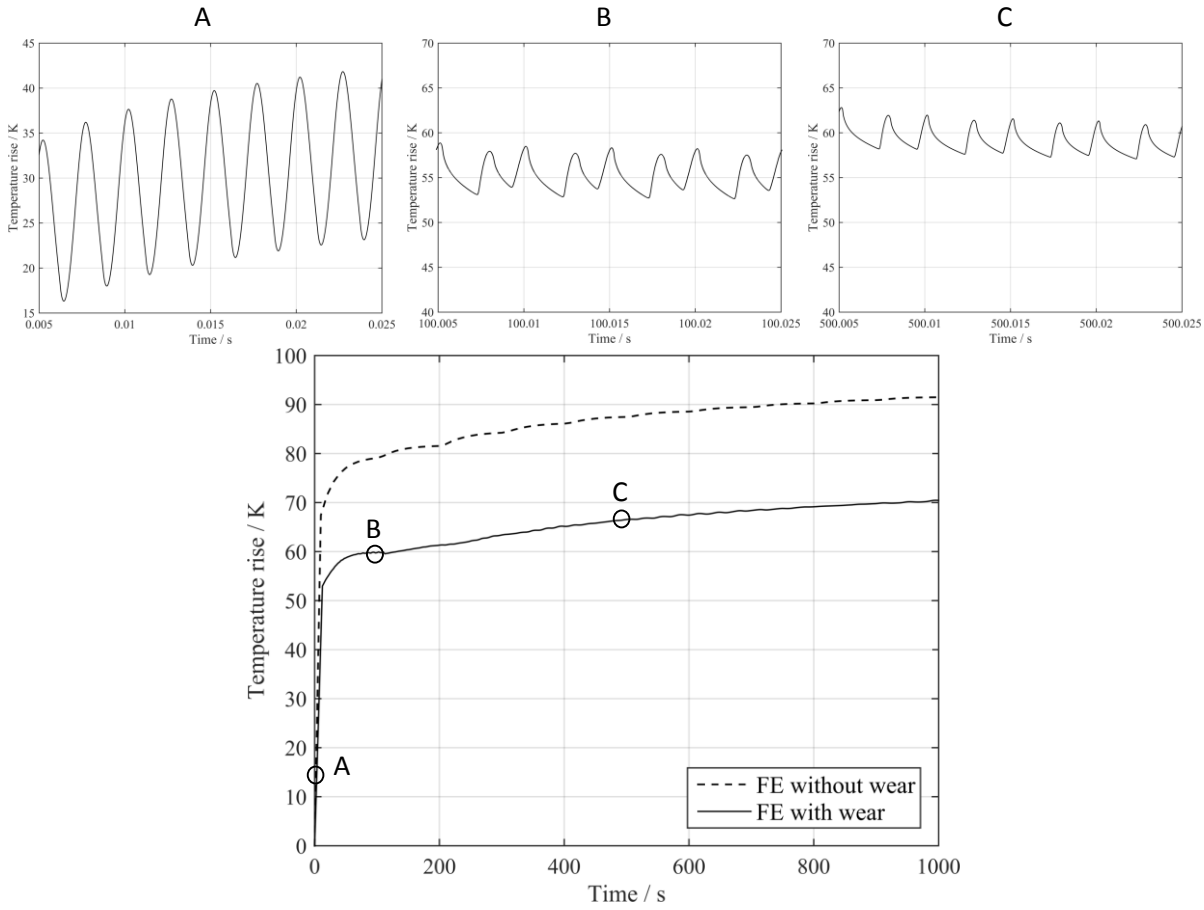

(b)

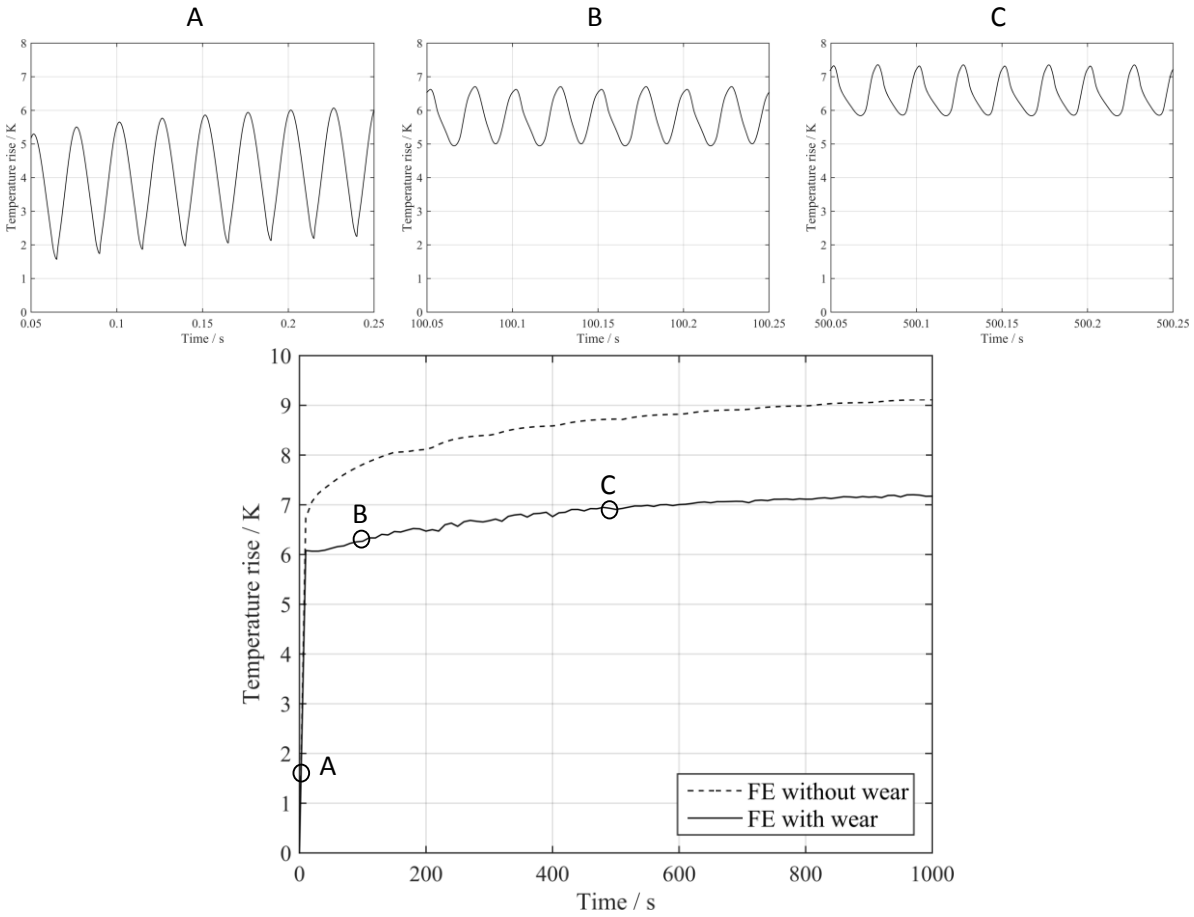

Figure 17 Demonstration of the geometrical effects of wear on the long term (1000 s) and in-cycle temperature rise at the centre of the wear scar calculated by FE model (*P* = 450 N, δ = 50 µm , μ = 0.61); (a) *f* = 200 Hz (b) *f* = 20 Hz

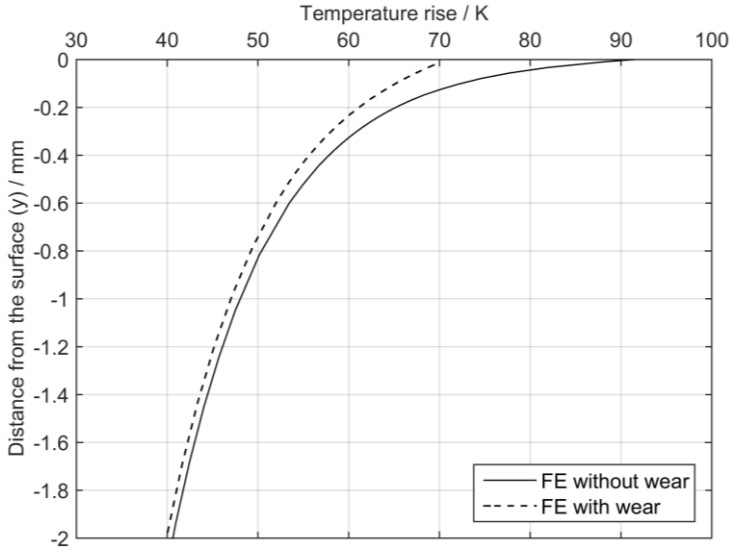

Figure 18 Comparison of the predicted centreline (*x* = 0) temperature rise as a function of distance below the surface from the FE model with and without geometry change at (*P* = 450 N, *f* = 200 Hz, δ = 50 µm, μ_E = 0.61, *t* = 1000 s)

Figure 17 shows the comparison of the FE model prediction of the temperature rise at the centre of the wear scar both with and without the geometrical changes associated with wear under both high (200 Hz) and low (20 Hz) frequencies for 1000 s. It can be seen that with the inclusion of wear in the

FE model, under the frequency of 200 Hz, the predicted mean surface temperature rises in the long term are about 20 K lower compared to the prediction based upon the initial contact geometry. However, this difference reduces dramatically below the contact as shown in Figure 18. The difference in temperature rise drops to about 2 K at the first experimental measurement point (y = 0.45 mm). When fretting is conducted at a lower frequency of 20 Hz, the geometry change only results in a reduction in surface temperature rise of about 3 K, but this is still quite significant as the overall temperature rise at this frequency is only around 10 K. In addition, the cyclic temperature variations before and after the development of the wear scar are also presented in Figure 17. It can be seen that for both high frequency and low frequency fretting tests, the cyclic temperature variations are much less significant as the wear scar develops (from about 20 K to less than 5 K for f = 200 Hz and from about 4 K to about 1 K for f = 20 Hz). It can be seen in Figure 19a that after the development of the wear scar, the contact pressure distribution is more uniform over a larger area on the surface. This will result in a reduction in the frictional power density dissipated and lead to the reduction of the maximum temperature rise at the centre of the wear scar. It should also be noted that for both frequencies, the effects of the geometry change on temperature rise does not vary for the majority of the simulation (after 100 s). It has shown in Figure 19b that the contact pressure at the centre of the wear scar dropped significantly at the beginning of the simulation. However, it reduced very slowly after 100 s which explains the constant difference in temperature rise.

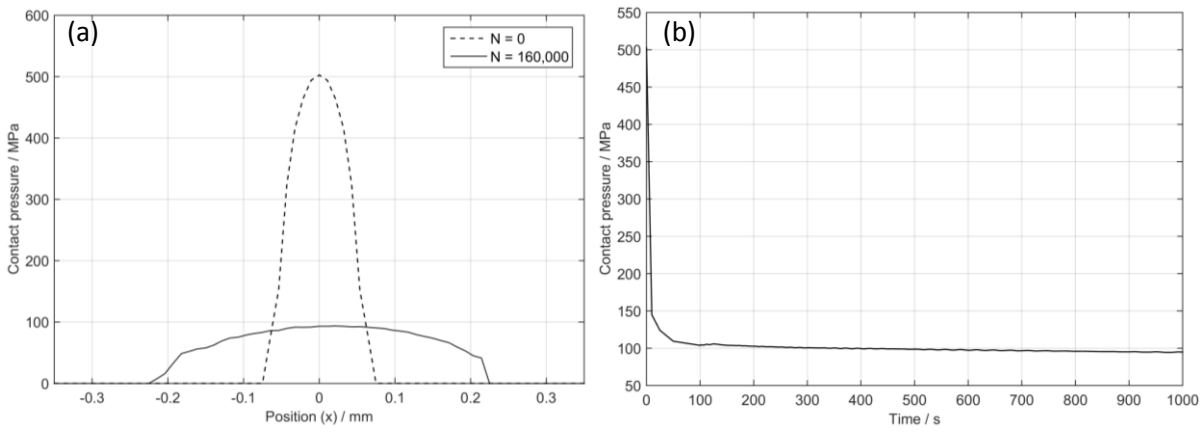

Figure 19 (a) Comparison of the contact pressure distribution on the surface with the FE wear model before and after wear is developed (b) Evolution of the contact pressure at the centre of the wear scar (P = 450 N, f = 200 Hz, δ = 50 µm, μ = 0.61)

5.2.2. Effects of the oxide layer

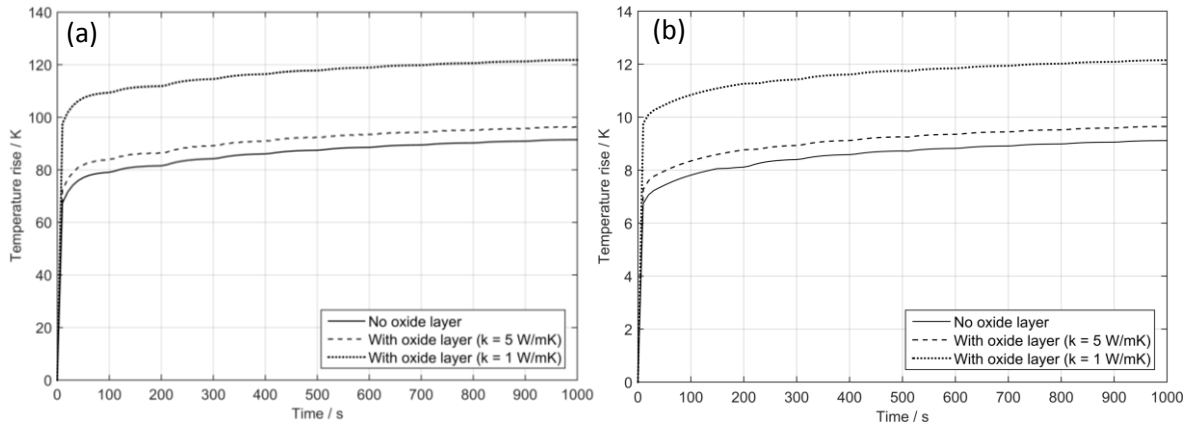

Figure 20 Comparision of the predicted temperature rise at the fixed origin with inclusion of oxide layer with different thermal properties for 1000 s (*P* = 450 N, δ = 50 µm, μ = 0.61, oxide layer thickness = 5 µm); (a) *f* = 200 Hz (b) *f* = 20 Hz

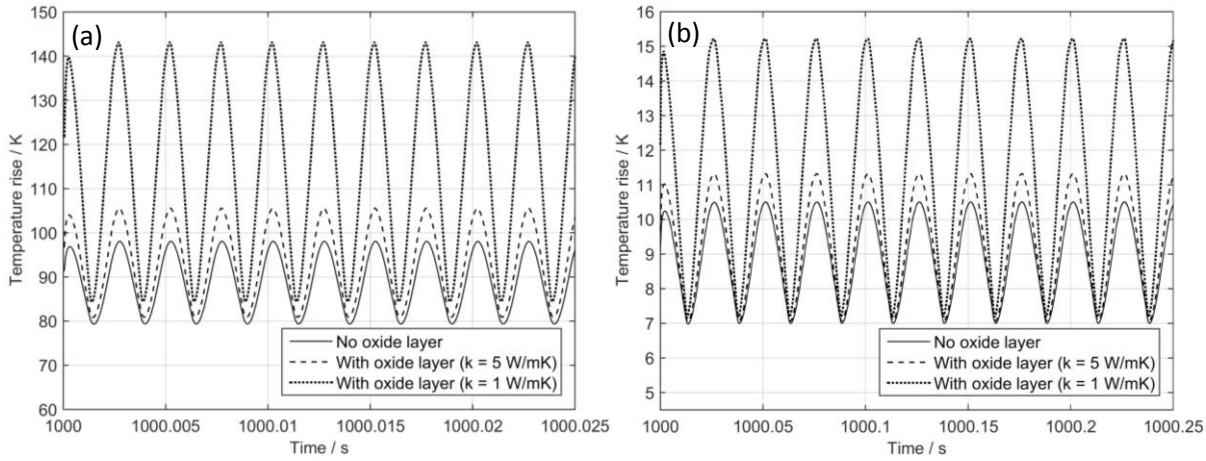

Figure 21 Comparision of the predicted temperature rise at the fixed origin with inclusion of oxide layer with different thermal properties (*P* = 450 N, δ = 50 µm, μ = 0.61, oxide layer thickness = 5 µm); (a) from 1000 s to 1000.025 s, *f* = 200 Hz (b) from 1000 s to 1000.25 s, *f* = 20 Hz

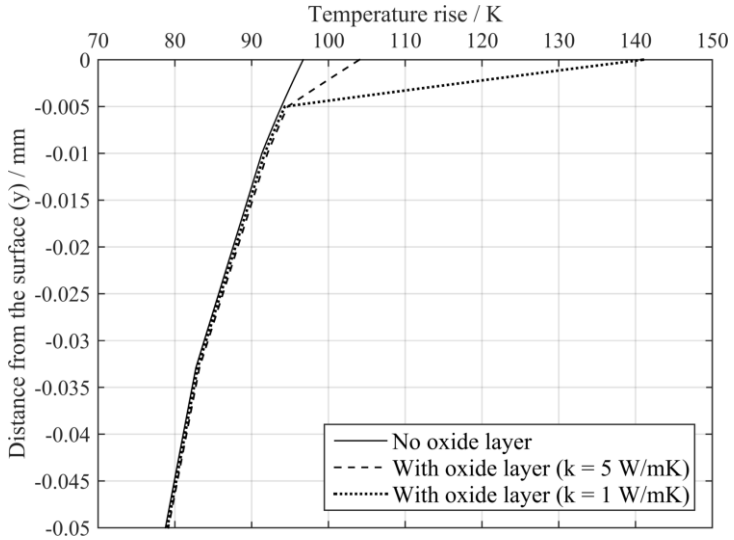

Figure 22 Comparison of the predicted centreline (*x* = 0) temperature rise as a function of distance below the surface at 1000.025 s from the FE model with inclusion of oxide layer with different thermal properties (*P* = 450 N, δ = 50 µm, *f* = 200 Hz, μ = 0.61, oxide layer thickness = 5 µm)

Figure 20 and Figure 21 shows the comparison of both mean temperature rise in long term (1000 s) and cyclic temperature rise for the few cycles after 1000 s at the fixed origin with the application of thermal conductivities of both 5 W m^{-1} K^{-1} and 1 W m^{-1} K^{-1} under 200 Hz and 20 Hz with a debris layer thickness of 5 µm (the mean debris layer thickness observed from the work of Pearson et al. [10]). It can be seen that both the mean temperature rise and the peak cyclic temperature rise in the contact are very sensitive to the thermal conductivity of the debris layer, despite the thickness of the oxide layer being only 5 µm. It can be seen (Figure 21) that when the thermal conductivity of the oxide layer was set to be 1 W m^{-1} K^{-1}, the peak temperature rise can be more than 50 K higher than that predicted when the oxide layer was excluded. With the increase of thermal conductivity from 1 W m^{-1} K^{-1} to 5 W m^{-1} K^{-1}, the role of the oxide in influencing the thermal field was significantly reduced. Figure 22 shows the predicted centreline (x = 0) temperature rise as a function of distance below the surface at 1000.025 s. It can be seen that the high temperature caused by the debris layer only exists in the debris layer itself, with the temperatures below the debris layer being almost the same for all three cases, indicating that the presence of the oxide layer will have little influence upon the mechanical property changes of the near-surface material.

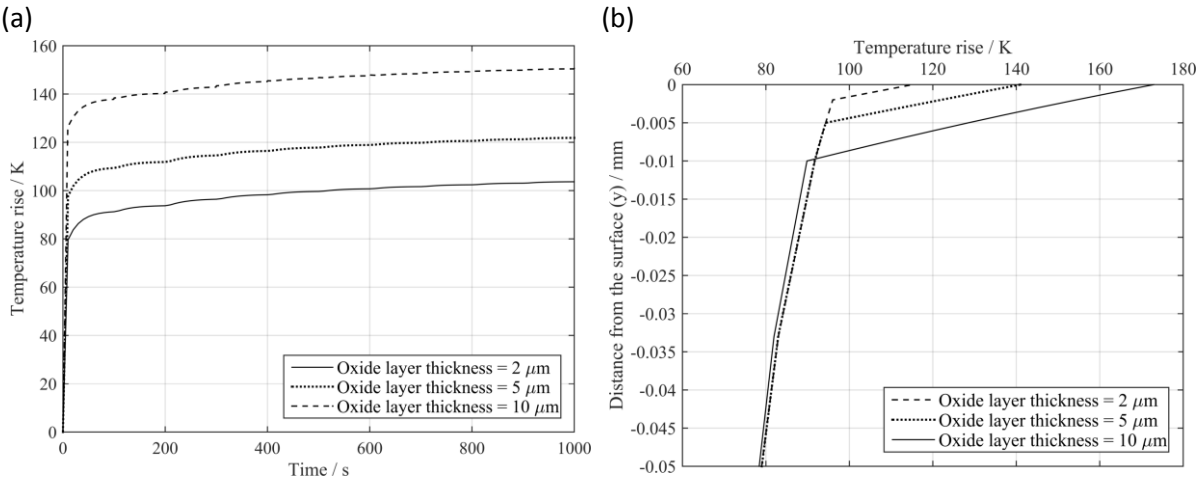

Figure 23 Comparision of the predicted temperature rise with inclusion of oxide layer with different layer thickness (P = 450 N, δ = 50 µm, μ = 0.61, f = 200 Hz, K = 1 W/mK) (a) at the fixed origin for 1000 s (b) along centreline (x = 0) below the surface at 1000.025 s

Figure 23 shows the effects of the thickness of the oxide layer on the near contact thermal field with the thermal conductivity of 1 W m^{-1} K^{-1} under 200 Hz. It can be seen that the increases in temperature at the fixed origin and across the oxide are larger with increasing oxide layer thickness. However, again, the presence of the oxide has little influence on the thermal field in the material just below the oxide layer itself.

5.3. Discussion

The significant reduction in both the average temperature rise and the amplitude of the cyclic temperature variation within the contact due to geometrical development is caused by the reduction of contact pressure, which directly related to the density of the heat input. The rapid reduction in the contact pressure at the early stage of the process is caused by the geometry change from a non-conforming cylinder-on-flat surface contact to a more conforming surface contact. However, the further development of the wear scar (past this initial change in geometry) has been shown to have small effects on the reduction of contact pressure. In addition, the effects of the

geometry changes to the thermal field have been shown only significant very close (less than 0.2 mm) to the contact (Figure 18).

The presence of the oxide layer has been shown to have significantly influence on both the average temperature rise and the maximum cyclic temperature rise in contact. However, its effect on the minimum temperature rise in a cycle and the temperature rise in the substrate itself is very small. Since the oxide layer is generally thin in a fretting contact (2 μm,5 μm and 10 μm in the model), its effects are only significant inside the layer itself when the power dissipation is high; the effects are very much influenced by the thermal properties and the thickness of the oxide layer as shown in Figure 22 and Figure 23.

As already stated, both the effects of geometry change and the presence of an oxide-based debris layer on the fretting induced thermal field are only significant in a small area very close to the contact. It is, therefore, not a surprise that the thermocouples did not capture these effects during the experiments; moreover, the experimentally measured temperature rises resulted in good a comparison with the predictions from the static constant heat source analytical model (despite the latter not including any of these changes caused by fretting wear), since the thermocouples are not in the surface zone which is affected the changes in geometry and debris formation associated with wear. However, the near-surface effects of geometry changes and debris formation on the surface temperature are of significant influence, since the physical process involved in fretting wear actually take place in this surface region. It is recognised that the rise of temperature induced by the frictional heat dissipation will influence the mechanical properties of both the bulk material and the oxide debris layer, leading to changes in plasticity and crack formation in this region. In the current model, the plasticity effect of both the bulk material and the oxide layer has been ignored in the FE model. Plastic deformation of the surface can result in the redistribution of the contact pressure, and thus influence the shape of the wear scar. Furthermore, temperature can also influence the oxidation rate and the formation of the debris layer which influence the fretting wear rate. Therefore, from the FE model developed in this paper, there is a potential to use the predicted temperature rise as an internal variable and thus increase the sophistication of existing FE-based wear models[30,36,37].

6. Conclusions

A FE model has been developed to predict the local temperature rise in fretting contact due to frictional power dissipation. The FE model has been benchmarked by showing good agreement with the solutions from analytical models; moreover, the results obtained from the analytical models were very comparable to those from corresponding experimental measurements. The FE model has been further applied to predict the effects of the development of wear scar and the presence of an oxide debris layer on the thermal fields generated in fretting. The geometrical development of the wear scar was found to significantly reduce the maximum temperature rise (and its cyclic variation) in the contact. The presence of an oxide debris layer was found to increase both the average temperature rise and peak temperature rise in the contact if the thermal conductivity of the layer is significantly lower than that of the base material. Both of these effects have been predicted to be localised very close to the contact, and thus cannot be captured by the thermocouples during the experiment.

Acknowledgements

The authors wish to thank the Taiho Kogyo Tribology Research Foundation, Toyota City, Japan for supporting an upgrade of the experimental facilities which have underpinned this work. The views expressed in this paper are those of the authors and not necessarily those of the Taiho Kogyo Tribology Research Foundation.

The authors would also like to thank the University of Nottingham for the award of the "Dean of Engineering Research Scholarship for International Excellence" to Xiaozhe Jin.

References

[1] O. Vingsbo, S. Söderberg, On fretting maps, Wear. 126 (1988) 131–147. doi:10.1016/0043-1648(88)90134-2.

[2] J.M. Dobromirski, Variables of Fretting Process: Are There 50 of Them?, in: Stand. Frett. Fatigue Test Methods Equip., ASTM, Philadelphia, 1992: pp. 60–66.

[3] H. Blok, The dissipation of frictional heat, Appl. Sci. Res. Sect. A. 5 (1955).

[4] M.F. Ashby, J. Abulawi, H.S. Kong, Temperature Maps for Frictional Heating in Dry Sliding, Tribol. Trans. 34 (1991) 577–587. doi:10.1080/10402009108982074.

[5] J. Wen, M.M. Khonsari, Transient temperature involving oscillatory heat source with application in fretting contact, J. Tribol. 129 (2007) 517. doi:10.1115/1.2736435.

[6] P.L. Hurricks, The fretting wear of mild steel from 200° to 500°C, Wear. 30 (1974) 189–212. doi:10.1016/0043-1648(74)90175-6.

[7] P.L. Hurricks, The fretting wear of mild steel from room temperature to 200°C, Wear. 19 (1972) 207–229. doi:10.1016/0043-1648(72)90304-3.

[8] R. Rybiak, S. Fouvry, B. Bonnet, Fretting wear of stainless steels under variable temperature conditions: Introduction of a "composite" wear law, Wear. 268 (2010) 413–423. doi:10.1016/j.wear.2009.08.029.

[9] T. Kayaba, A. Iwabuchi, The fretting wear of 0.45% C steel and austenitic stainless steel from 20 to 650 °C in air, Wear. 74 (1981) 229–245. doi:10.1016/0043-1648(81)90165-4.

[10] S.R. Pearson, P.H. Shipway, J.O. Abere, R.A.A. Hewitt, The effect of temperature on wear and friction of a high strength steel in fretting, Wear. 303 (2013) 622–631. doi:http://dx.doi.org/10.1016/j.wear.2013.03.048.

[11] C. Colombie, Y. Berthier, A. Floquet, L. Vincent, M. Godet, Fretting: load carrying capacity of wear debris, J. Tribol. Trans. ASME. 106 (1984) 194–201. doi:10.1115/1.3260881.

[12] I. Feng, H.H. Uhlig, Fretting corrosion of mild steel in air and in nitrogen, J. Appl. Mech. ASME. 21 (1954) 395–400.

[13] H.H. Uhlig, Mechanism of fretting corrosion, J. Appl. Mech. ASME. 21 (1954) 401–407.

[14] A.R. Warmuth, P.H. Shipway, W. Sun, Fretting wear mapping: the influence of contact geometry and frequency on debris formation and ejection for a steel-on-steel pair, Proc. R. Soc. London A Math. Phys. Eng. Sci. 471 (2015). doi:10.1098/rspa.2014.0291.

[15] J. Jaeger, Moving sources of heat and the temperature of sliding contacts, J. Proc. Roy. Soc. New South Wales. (1942). http://ci.nii.ac.jp/naid/10008203948/ (accessed May 25, 2014).

[16] J.F. Archard, The temperature of rubbing surfaces, Wear. 2 (1959) 438–455. doi:10.1016/0043-1648(59)90159-0.

[17] X. Tian, J.F.E. Kennedy, Maximum and Average Flash Temperatures in Sliding Contacts, J. Tribol. 116 (1994) 167–174. doi:10.1115/1.2927035.

[18] J.A. Greenwood, J.B.P. Williamson, Contact of Nominally Flat Surfaces, Proc. R. Soc. A Math. Phys. Eng. Sci. 295 (1966) 300–319. doi:10.1098/rspa.1966.0242.

[19] J.A. Greenwood, A.F. Alliston-Greiner, Surface temperatures in a fretting contact, Wear. 155 (1992) 269–275. doi:10.1016/0043-1648(92)90086-N.

[20] M.H. Attia, N.S. D'Silva, Effect of mode of motion and process parameters on the prediction of temperature rise in fretting wear, Wear. 106 (1985) 203–224. doi:10.1016/0043-1648(85)90110-3.

[21] M. Helmi Attia, F. Camacho, Temperature field in the vicinity of a contact asperity during fretting, ASME-PUBLICATIONS-PED. 67 (1993) 51.

[22] M.H. Attia, M.M. Yovanovich, A model for predicting the thermal constriction resistance in fretting, Proc. ASME Symp. Contact Probl. Surf. Interact. Manuf. Tribol. Syst. 67 (1993) 63–74.

[23] H. Attia, Thermal constriction phenomenon in fretting: Theory and implications, Tribol. Int. 44 (2011) 1352–1363. doi:10.1016/j.triboint.2011.04.022.

[24] K.L. Johnson, Contact Mechanics, Cambridge University Press, Cambridge, 1987.

[25] H.S. Carslaw, J.C. Jaeger, Conduction of heat in solids, Oxford Clarendon Press, London, 1959.

[26] M.H. Attia, A. Cameron, L. Kops, Distortion in Thermal Field Around Inserted Thermocouples in Experimental Interfacial Studies, Part 4: End Effect, J. Manuf. Sci. Eng. 124 (2002) 135. doi:10.1115/1.1419199.

[27] I.. McColl, J. Ding, S.. Leen, Finite element simulation and experimental validation of fretting wear, Wear. 256 (2004) 1114–1127. doi:10.1016/j.wear.2003.07.001.

[28] X. Jin, P.H. Shipway, W. Sun, The role of frictional power dissipation (as a function of frequency) and test temperature on contact temperature and the subsequent wear behaviour in a stainless steel contact in fretting, Wear. 330-331 (2015) 103–111. doi:10.1016/j.wear.2015.02.022.

[29] J. Jiang, F.H. Stott, M.M. Stack, The role of triboparticulates in dry sliding wear, Tribol. Int. 31 (1998) 245–256. doi:10.1016/S0301-679X(98)00027-9.

[30] N.M. Everitt, J. Ding, G. Bandak, P.H. Shipway, S.B. Leen, E.J. Williams, Characterisation of fretting-induced wear debris for Ti-6Al-4 V, Wear. 267 (2009) 283–291. doi:10.1016/j.wear.2008.12.032.

[31] M. Takeda, T. Onishi, S. Nakakubo, S. Fujimoto, Physical Properties of Iron-Oxide Scales on Si-Containing Steels at High Temperature, Mater. Trans. 50 (2009) 2242–2246. doi:10.2320/matertrans.M2009097.

[32] M. Torres, R. Colás, A model for heat conduction through the oxide layer of steel during hot rolling, J. Mater. Process. Technol. 105 (2000) 258–263. doi:10.1016/S0924-0136(00)00569-0.

[33] S.S. Shinde, K.Y. Rajpure, Investigation of structural, morphological, luminescent and thermal

properties of combusted aluminium-based iron oxide, J. Solid State Chem. 183 (2010) 2886–2894. doi:10.1016/j.jssc.2010.09.035.

[34] R. Endo, T. Yagi, M. Ueda, M. Susa, Thermal Diffusivity Measurement of Oxide Scale Formed on Steel during Hot-rolling Process, ISIJ Int. 54 (2014) 2084–2088. doi:10.2355/isijinternational.54.2084.

[35] J. Mørgaard, W.W. Smeltzer, Thermal Conductivity of Magnetite and Hematite, J. Appl. Phys. 42 (1971) 3644. doi:10.1063/1.1660785.

[36] J. Ding, I.R. McColl, S.B. Leen, P.H. Shipway, A finite element based approach to simulating the effects of debris on fretting wear, Wear. 263 (2007) 481–491. doi:10.1016/j.wear.2006.12.056.

[37] J. Ding, S.B. Leen, E.J. Williams, P.H. Shipway, A multi-scale model for fretting wear with oxidation-debris effects, Proc. Inst. Mech. Eng. Part J J. Eng. Tribol. 223 (2009) 1019–1031. doi:10.1243/13506501JET589.